

ORDER, DISORDER, AND PHASE TRANSITION
IN CONDENSED SYSTEM

Schottky Anomalies in the Low-Temperature Specific Heat of $\text{YBa}_2\text{Cu}_3\text{O}_y$ HTSC

L. G. Mamsurova^{a,*}, N. G. Trusevich^a, S. Yu. Gavrilkin^b,
I. V. Mamsurov^a, and L. I. Trakhtenberg^{a,c,**}

^a *Semenov Institute of Chemical Physics, Russian Academy of Sciences, Moscow, 119991 Russia*

^b *Lebedev Physical Institute, Russian Academy of Sciences, Moscow, 119991 Russia*

^c *Moscow State University, Moscow, 119991 Russia*

**e-mail: mamsurova@chph.ras.ru*

***e-mail: litrakh@gmail.com*

Received August 9, 2018; revised November 2, 2018; accepted November 8, 2018

Abstract—The evolution of the Schottky anomalies in the temperature dependence of the specific heat (in the temperature range $T = 2\text{--}10$ K and the magnetic field range $H = 0\text{--}9$ T) of polycrystalline $\text{YBa}_2\text{Cu}_3\text{O}_y$ HTSCs is studied when the oxygen content in coarse-crystalline samples changes and when the degree of structural disordering in optimally doped fine-crystalline samples of the same compound changes. The number of paramagnetic centers with uncompensated spin moments, which generate the Schottky anomalies, and the splitting of the lower energy levels are estimated. A correlation between these parameters and both the number of oxygen vacancies in chain planes and the method of oxygen ordering in chains is found. The experimental data are compared with the results of studying the magnetic susceptibility at $T > T_c$ in the same samples. Based on this comparison, we can conclude that the nature of the Schottky centers is related to the formation of paramagnetic centers at breaks in the $\text{Cu1}\text{--}\text{O4}$ copper–oxygen chains in the basal planes of the crystal structure.

DOI: 10.1134/S1063776119030099

1. INTRODUCTION

Cuprate HTSCs are known to be d -wave superconductors, which means that their gap function has nodes at the Fermi surface where the superconducting gap tends toward zero. As a result, some quasiparticle states near the nodes can be reached at the lowest temperatures and determine an electronic contribution to the specific heat. Thus, the study of the low-temperature specific heat of HTSC gives direct bulk information on the behavior of the superconducting gap near the nodes and, hence, is of special interest. In particular, low-temperature specific heat turned out to be helpful for solving the problem of identifying the d -wave pairing symmetry in HTSC [1].

The earlier investigations (see, e.g., [2, 3]) of the low-temperature specific heat of $\text{YBa}_2\text{Cu}_3\text{O}_y$ HTSC showed the presence of various electronic contributions to the specific heat along with lattice contributions. The node contributions of low-energy excitations were of deep interest. A finite slope of the V-like gap near the nodes was found to cause a linear dependence of low-energy density of states $N(\epsilon) \propto |\epsilon - \epsilon_f|$. As a consequence, the specific heat at temperature $T \rightarrow 0$ K in the absence of a magnetic field turns out to be proportional to αT^2 . In a sufficiently strong mag-

netic field, the quadratic term αT^2 is suppressed and replaced by another temperature-linear node term $A_v \sqrt{H} T$, where A_v reflects the nodal gap slope in the direction perpendicular to the line of nodes [1, 3]. This term was predicted by Volovik [4]. He showed that a supercurrent around vortex cores in the mixed state leads to the Doppler shift of a quasiparticle excitation spectrum. This shift gives a noticeable effect near the d -wave nodes, where it is comparable with the disappearing superconducting gap. As a result, additional quasiparticle states, which also contribute to the specific heat, become accessible.

On the whole, the specific heat of $\text{YBa}_2\text{Cu}_3\text{O}_y$ HTSC at $H = 0$ and $T < 10$ K was shown to be described well by the expression [2, 3]

$$C(T) = \gamma(0)T + \alpha T^2 + \beta T^3 + \delta T^5 + A_2/T^2, \quad (1)$$

in the presence of a magnetic field, the specific heat is

$$C(T) = [\gamma(0) + A_v \sqrt{H}]T + \beta T^3 + \delta T^5 + C_{\text{Sch}}. \quad (2)$$

As follows from Eqs. (1) and (2), they contain the node terms noted above, two lattice terms (Debye term proportional to T^3 , the term that takes into account the anharmonicity of phonon vibrations and

is proportional to T^5), and two additional electronic contributions. First, it is temperature-linear term $\gamma(0)T$ at $H = 0$, which indicates the existence of a noticeable amount of nonsuperconducting quasiparticle states at low temperatures. (The nature of this term has not been revealed reliably to date. It is usually inherent in metals and should not be observed in ideal superconductors. The data obtained in [5, 6] point to a relation between this term and the degree of structural disordering.) Second, it is the contribution to the specific heat that has the form of Schottky anomalies, C_{Sch} . At $H = 0$, the maximum of such an anomaly is at ultralow temperatures (less than 2 K); therefore, only its “tail” proportional to T^{-2} is visible at $T > 2$ K.

As was shown in [5, 6], it is $\text{YBa}_2\text{Cu}_3\text{O}_y$ HTSC that exhibits unusually high Schottky anomalies, and these anomalies have not been detected at all in other HTSCs, e.g., LaSrCuO or BiSrLaCuO . However, the existence of Schottky anomalies substantially makes it difficult to obtain reliable quantitative information on the important terms in Eqs. (1) and (2) such as the nodal terms (since it is these terms that reflect the key HTSC parameters that determine the slope of the superconducting gap near the d -wave nodes, in particular, the superconducting transition temperature) and the “mysterious” linear term $\gamma(0)T$ noted above.

It should be noted that, despite a series of works [7–9] focused on the Schottky anomalies noted above, the cause why these anomalies exist in $\text{YBa}_2\text{Cu}_3\text{O}_y$ HTSC and are high has not yet been revealed. For example, the authors of [7] showed that the concentration of Schottky paramagnetic centers increases with decreasing oxygen content y ; however, in contrast to expectations, this increase is not comparable with an increase in the oxygen vacancy concentration and is lower by two orders of magnitude. As a result, it is still unclear how 100 oxygen vacancies generate one paramagnetic center.

As was noted in [8], the nature of the Schottky centers is still unclear, and it is usually described by the paramagnetic centers related to the uncompensated spin ($s = 1/2$) moments of copper. As an example, the experiments [10] on the substitution of Zn and Cr atoms for copper atoms were presented. It was shown that a Zn atom actually removes the spin moment of copper and the substitution of a Cr atom for copper leads to the Schottky anomaly in low fields, which is well described by a two-level system with $g = 2$. As a result, the authors of [10] concluded that the Schottky anomalies were caused by disorder-induced paramagnetic centers, since the effect increases with the disorder.

The authors of [9] studied weakly doped (non-superconducting) $\text{YBa}_2\text{Cu}_3\text{O}_{6+x}$ ($x = 0.28, 0.32, 0.34$) samples and showed that the total specific heat at low temperatures is also determined by local excitations in the copper–oxygen (Cu1–O4) chains. They demonstrated the scenario of appearance of a Schottky center

from a five-ion complex in the chains and noted that a complex with an odd number of copper ions (Cu1) can only form the Schottky anomaly. In addition, they calculated the energy structure of the divalent copper ion, which is characterized by spin ($s = 1/2$) and orbital ($l = 2$) moments. This structure forms due to the action of a crystal field, a spin–orbit interaction, and an applied magnetic field. As a result, the authors of [9] obtained a calculated temperature dependence of the specific heat, which well described the experimental curve; and good agreement between experimental and calculated data has not been achieved for these samples in terms of a simple two-level system.

The purpose of this work is to study and compare $\text{YBa}_2\text{Cu}_3\text{O}_y$ samples with various microstructures in order to obtain information on the Schottky parameters and to reveal the nature of the Schottky centers in this compound.

2. EXPERIMENTAL

We analyzed polycrystalline $\text{YBa}_2\text{Cu}_3\text{O}_y$ samples belonging to two different groups.

The first group consisted of coarse-grained crystalline equilibrium samples (synthesized by a conventional solid-phase method) with the following oxygen contents: $y = 7.00$ in sample 1 and $y = 6.63$ in sample 2. The second group contained optimally doped ($y \approx 6.92 \pm 0.03$) fine-crystalline samples with various degrees of nanoscale structural heterogeneity and, correspondingly, various average crystallite sizes ($\langle D \rangle$) in micron and submicron ranges: $\langle D \rangle \approx 2 \mu\text{m}$ in sample 1', $\langle D \rangle \approx 1 \mu\text{m}$ in sample 2', and $\langle D \rangle \approx 0.4 \mu\text{m}$ in sample 3'.

The samples of the second group were prepared using mechanochemistry technique [11, 12] under nonequilibrium conditions related to high-rate structure formation at low annealing temperatures (T_{ann}) and short annealing times (τ_{ann}). The final microstructures of the samples substantially depended on the degree of activation of a mixture of initial components (CuO, BaO, Y_2O_3) and its reactivity. When the mechanically activated mixture was placed in a heated furnace, an orthorhombic structure crystallized in a time much shorter than 1 h. The lower the structure formation temperature T_{ann} , the smaller the crystallite size $\langle D \rangle$, and the lower the degree of cation ordering, since T_{ann} is the main parameter of the solid-state diffusion process in which cations are ordered. As a result, changing the high-temperature treatment conditions, we can control both the average crystallite size $\langle D \rangle$ and the degree of cation ordering in the $\text{YBa}_2\text{Cu}_3\text{O}_y$ system, which were found to be interrelated [13].

Thus, we can stabilize states with incomplete atomic ordering and solve the problem of controlled structural disordering. As was shown in [13], the parameter that adequately reflects the degree of struc-

tural disordering in the fine-crystalline samples is average crystallite size $\langle D \rangle$.

The neutron-diffraction studies [13] found the main type of defects in mechanically activated samples, namely, the mutual substitution of Y^{3+} and Ba^{2+} cations and the corresponding oxygen redistribution. It was found that the smaller the average crystallite size, the larger the number of defect unit cells with mutually substituted cations in samples (see Fig. 6 in [13]). The oxygen content in the chain planes increases and the occupancy of the oxygen O5 sites (which should be empty in an ideal situation) becomes anomalously high, whereas the oxygen content in the chain O4 sites remains almost the same (see Fig. 5 in [13]). The same effect was detected with Mössbauer spectroscopy [14, 15]. As a result, unit cell parameters a and c in the fine-crystalline samples change significantly as compared to those in the samples fabricated under equilibrium conditions. However, parameter b , along which copper–oxygen chains are arranged, remains almost the same (see Fig. 4 in [13]). It should be noted that the defects detected in the fine-crystalline $YBa_2Cu_3O_y$ samples were not detected in the coarse-crystalline samples, and their existence was detected in thin films of the given compound [16, 17].

As was shown in [13], the smaller the average crystallite size, the smaller the structural homogeneity domain size. In sample 3' ($\langle D \rangle \approx 0.4 \mu\text{m}$), this domain size is about 10 \AA , which is comparable with the coherence length ($\xi(T=0) \approx 15 \text{ \AA}$) and is substantially smaller than London's penetration depth λ of magnetic field ($\lambda(T=0) \approx 0.15 \mu\text{m}$). As a result, the magnetic characteristics (magnetization, magnetic susceptibility) change when $\langle D \rangle$ decreases [13, 18].

All samples from the second group were identically saturated with oxygen. As a result, the values of T_c in them were almost the same, $T_c = 91.4 \pm 0.3 \text{ K}$ (see Fig. 3 in [5]). However, as follows from [5], the specific heat jump $\Delta C/T$ decreases with decreasing $\langle D \rangle$, which indicates the suppression of the density of superconducting quasiparticle states when the degree of structural disordering increases [5].

Information on $\langle D \rangle$ was obtained from scanning electron microscopy data and was then refined by measuring dynamic magnetic susceptibility χ_{ac} in ac magnetic fields [13]. Oxygen index y was determined by iodometric titration accurate to ± 0.03 . The specific heat was measured by a relaxation method on a PPMS Quantum Design device in the temperature range $T = 2\text{--}10 \text{ K}$ at magnetic fields $H = 0\text{--}9 \text{ T}$. Static magnetic susceptibility in the normal state (at $T \geq T_c$) was measured using a Faraday balance on an Oxford Instruments device.

3. RESULTS AND DISCUSSION

Figure 1 shows the experimental results on measuring the specific heat of sample 2 in various magnetic

fields in the $C/T - T^2$ coordinates in the low-temperature range under study. To a first approximation, the specific heat is seen to be determined by the sum of two main contributions, namely, the lattice and Volovik node contributions. The lattice contribution in these coordinates provides field-independent slopes of the curves. At high temperatures, the field-dependent electronic term (which is proportional to $A_V \sqrt{H} T$) shifts the curves parallel to each other when the field increases. The low-temperature rises are Schottky anomalies. Strong fields are seen to make the excess of the Volovik contribution over the Schottky specific heat more pronounced.

When plotting experimental results in various coordinates and in various magnetic field ranges, we can find the desired coefficients before all terms in Eqs. (1) and (2) as fitting parameters, including the number of Schottky centers n_{Sch} and the gap Δ between the lower energy levels.

For example, it is convenient to determine lattice parameters β and δ from the results presented in the $C/T - T$ coordinates at rather high magnetic fields $H \geq 1 \text{ T}$ (Fig. 2). In this case, coefficient α of quadratic-field term αT^2 is almost zero [1], and the contribution of Schottky anomalies at $T > 7 \text{ K}$ is minimal. Retaining the obtained lattice parameters, we analyze the results obtained for all magnetic fields to determine parameter $\gamma(H) = \gamma(0) + A_V \sqrt{H}$ (see inset to Fig. 2) and Schottky parameters n_{Sch} and Δ (see below). The solution of this problem was promoted by the fact that term $\gamma(H)$ in the $C/T - T$ coordinates is temperature independent and is well described by the root dependence on magnetic field predicted by Volovik [4] for d -wave superconductors (see inset to Fig. 2). The retained temperature-dependent part of Eq. (2) fully belongs to term C_{Sch} .

Figures 3 and 4 (for samples having different oxygen contents and degrees of structural disordering, respectively) show the temperature dependences of specific heat C/T in a magnetic field $H = 8 \text{ T}$ after the lattice contributions βT^3 and δT^5 and the temperature-linear electronic contribution $\gamma(H)T$ are subtracted. This subtraction leads to the curves the shape of which corresponds to Schottky anomalies. This is indicated by the fitting curves calculated by the Schottly formula

$$C_{\text{Sch}} = n_{\text{Sch}} R \left(\frac{\Delta}{k_B T} \right)^2 \frac{\exp(\Delta/k_B T)}{[1 + \exp(\Delta/k_B T)]^2}, \quad (3)$$

where R is the Rydberg constant; n_{Sch} is the number of Schottky centers; and Δ is the gap between the lower energy levels,

$$\Delta = 2gS\mu_B H_{\text{eff}}, \quad H_{\text{eff}} = \sqrt{H_{\text{appl}}^2 + H_{\text{int}}^2},$$

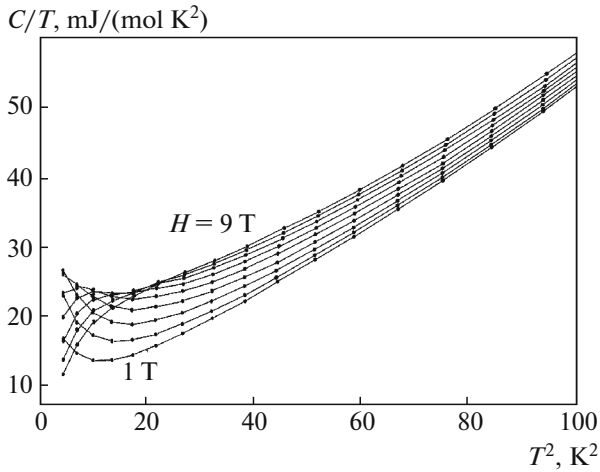


Fig. 1. Low-temperature specific heat C/T of $\text{YBa}_2\text{Cu}_3\text{O}_y$ HTSC (sample 2) vs. T^2 in a magnetic field $H = 1, 2, 3, 4, 5, 6, 7, 8,$ and 9 T. The solid curves connecting experimental points are plotted for clarity.

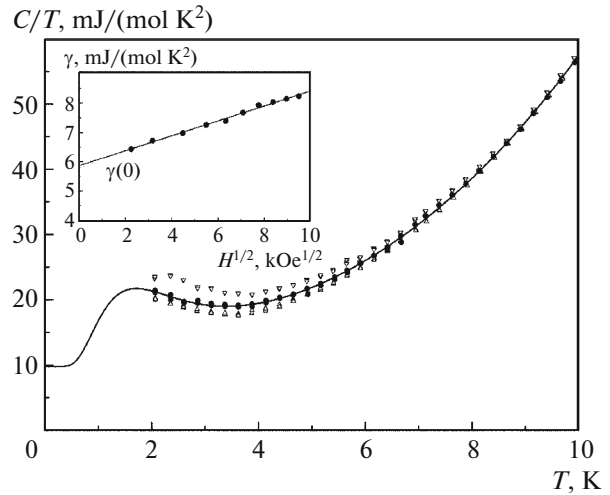


Fig. 2. Specific heat C/T of sample 3' vs. temperature: (points) experimental values, (solid symbols) $H = 1$ T, (open symbols) $H = 0$ (lower curve) and 2 T (upper curve), and (solid curve) fitting by Eq. (2). (inset) Coefficient before the temperature-linear contribution to the specific heat $\gamma(H)$ vs. \sqrt{H} . (solid curve) Fitting by the expression $\gamma(H) = \gamma(0) + A\sqrt{H}$.

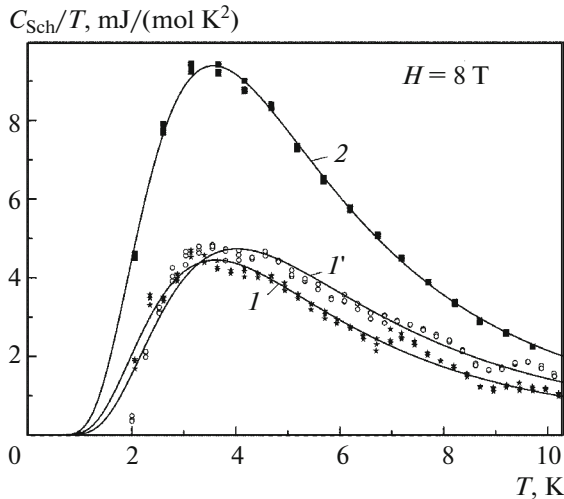


Fig. 3. Schottky anomalies in a magnetic field $H = 8$ T for samples with various oxygen contents: (1) sample 1 ($y = 7$), (1') sample 1' ($y = 6.92$), and (2) sample 2 ($y = 6.63$). (symbols) Experimental values and (solid curves) calculation by Eq. (3).

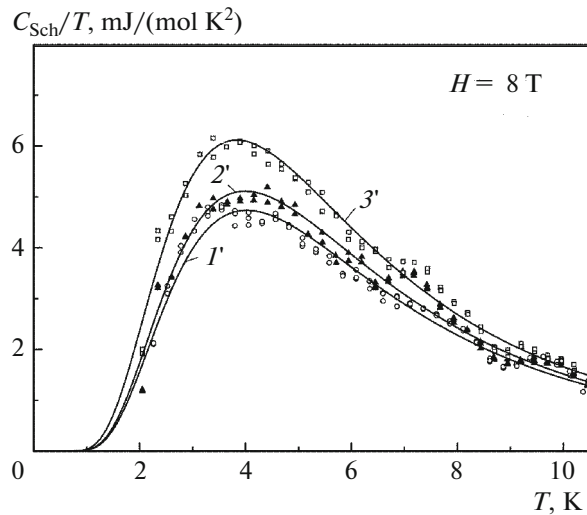


Fig. 4. Schottky anomalies in a magnetic field $H = 8$ T for samples with various average crystallite sizes $\langle D \rangle$ ((1') 2, (2) 1, (3') $0.4 \mu\text{m}$) and various degrees of structural ordering: (symbols) experimental values and (solid curves) calculation by Eq. (3).

where H_{appl} and H_{int} are the applied and internal magnetic fields, respectively. Adjustable parameters n_{Sch} (per unit cell) and Δ for all samples are shown in Fig. 5.

It is known [8] that specific heat C_{Sch} increases exponentially with temperature at low temperatures, where $k_{\text{B}}T \ll 2gS\mu_{\text{B}}H_{\text{eff}}$. At high temperatures ($k_{\text{B}}T \gg 2gS\mu_{\text{B}}H_{\text{eff}}$), the specific heat decreases as T^{-2} ; as a result, a peak forms at intermediate temperatures. An

applied magnetic field decreases the peak amplitude, shifts the peak temperature, and increases the peak width (Fig. 6 shows the dynamics of the behavior of Schottky anomalies in sample 2). The contribution of Schottky anomalies becomes negligibly small at very high fields.

As is seen in Fig. 5a, the number of Schottky centers n_{Sch} increases with the field. This fact is clear: the lower energy levels are split in a zero applied field

under the action of only internal fields H_{int} . Applied magnetic field H_{appl} creates additional splitting, increasing the number of Schottky centers.

These results demonstrate that the degenerate states in one group of samples (more equilibrium) undergo splitting due to the action of internal fields only in one-third of the centers. In the other group (structurally disordered), two-thirds of the maximum number of centers undergo splitting. The maximum values of n_{Sch} correlate with both the oxygen content and the degree of structural disordering. This finding needs a separate theoretical consideration. We only assume that in the structurally disordered samples, this difference is caused by the additional oxygen atoms that occupy the O5 sites in the basal planes, which should be free in an ideal situation (see Fig. 6 in [13]). As is seen in Fig. 5a, the number of Schottky centers is saturated only in high fields $H > 3$ T.

As is seen in Fig. 3, the Schottky anomaly height at the maximum obviously correlates with oxygen content y : the lower the oxygen content (i.e., the larger the number of oxygen vacancies), the higher the anomaly maximum. It is also seen in Fig. 5a that an increase in the number of oxygen vacancies in the samples increases the number of Schottky centers n_{Sch} . A decrease in the oxygen content in samples 1 and 2 of the first group causes a more than twofold increase in the number of Schottky centers $n_{\text{Sch}}(H)$, and Δ (temperature position of the maximum) remains unchanged (also see Fig. 5b). Therefore, we can conclude that the Schottky centers in these equilibrium samples have a similar nature.

As for oxygen content y , sample I' occupies an intermediate position. However, the maximum in the curve of this sample is slightly shifted toward high temperatures. The shift of the maximum corresponds to the increase in effective field H_{eff} that splits a certain level due to an increase in H_{int} .

In Figs. 4 and 5, we compare the Schottky anomalies in the structurally disordered samples of the second group and find that Schottky parameters n and Δ are also sensitive to the degree of structural disordering: the higher the degree of structural disordering, the larger the number of Schottky centers in a sample. The maxima of all three curves in Fig. 4 are seen to be located at approximately the same temperature. This finding agrees with the fact that level splitting Δ is approximately the same for the structurally disordered samples, which indicates general nature of the defects in all three samples of the second group (see Fig. 5b).

Figure 7 shows the electronic contributions to the specific heat for all samples in the absence of a magnetic field ($H = 0$). In this case, the lower energy levels are split only due to internal fields and interactions, which also causes Schottky anomalies. These anomalies take place at lower temperatures, so that only their tails are visible at $T > 2$ K.

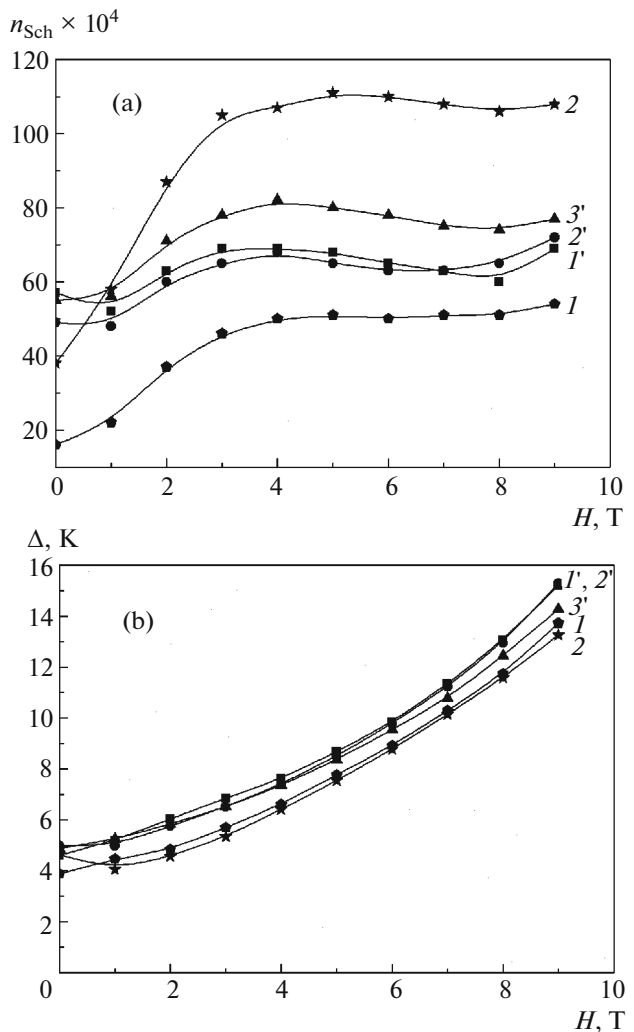


Fig. 5. Schottky parameters (a) n_{Sch} and (b) Δ vs. magnetic field H for all samples.

As follows from the curves in Fig. 7, the results obtained for all samples are naturally divided into two groups. The tails in each group almost coincide and the tails in different groups are substantially different. This effect is formally caused by the differences in the values of parameter $\gamma(0)$ for each group, since the temperature-independent coefficients of the linear terms of the specific heat turn out to be “supports” on which the temperature-dependent Schottky anomalies are located. However, the true cause of the differences between the two groups of samples is the difference between the natures of these anomalies. Based on our results, we assume that the Schottky centers in the first group of samples (sample 1, 2) are mainly related to the oxygen vacancies in the copper–oxygen chains in the basal planes, and this mechanism of formation of Schottky centers in the second group of samples (sample 1', 2', 3') is supplemented by another mechanism, namely, structural disordering. This mechanism

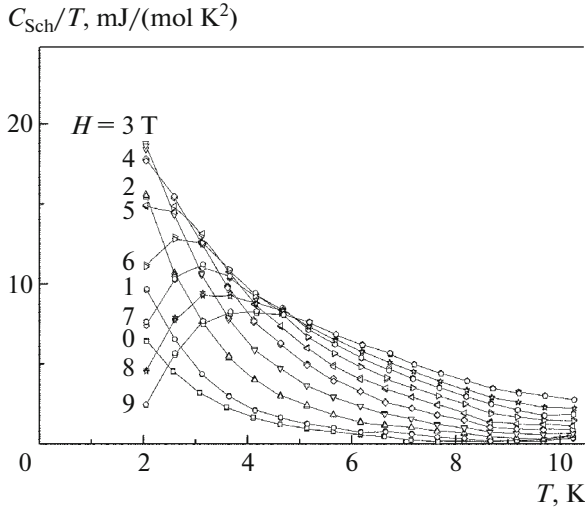


Fig. 6. Schottky anomalies in sample 2 vs. temperature for various magnetic fields. Numerals at the curves indicate the magnetic fields in tesla.

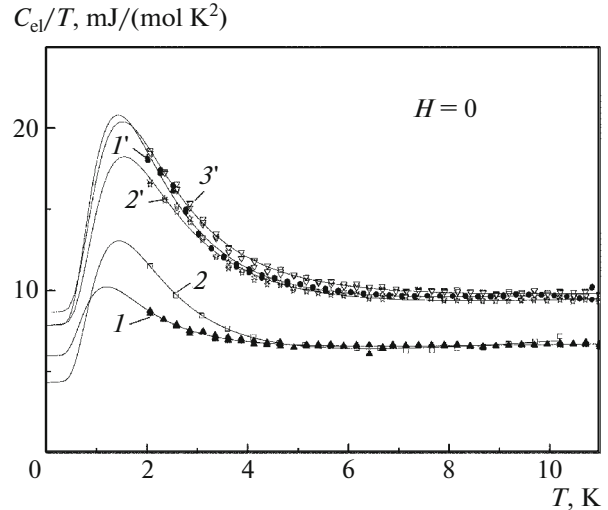


Fig. 7. Electronic contributions to the specific heat for all samples at $H = 0$. Numerals at the curves indicate sample numbers.

is known to involve other crystal structure layers: as noted above, mutual cation substitution leads to oxygen redistribution between the layers [13].

As follows from the aforesaid, all samples have Schottky centers, the lower energy levels of which are split by internal fields even at $H = 0$. An applied magnetic field enhances this splitting.

Our data agree with the assumption that the Schottky centers are represented by certain paramagnetic centers with uncompensated spin moments.

It is interesting that, although the numbers of Schottky centers n_{Sch} in the samples at $H = 0$ are different, they do not exceed six centers per 1000 unit cells!

The nature of the Schottky centers can be clarified if we compare our results with the study [19] of the magnetic susceptibility of the normal state (at $T > T_c$) in equilibrium coarse-crystalline $\text{YBa}_2\text{Cu}_3\text{O}_y$ samples with various values of y , which included samples 1 and 2 considered in this work.

Figure 8 shows the experimental results obtained in [19]. Curve 1 corresponds to the most strongly doped sample (sample 1); at $T > 120$ K, it demonstrates the susceptibility of the Pauli type, i.e., almost temperature-independent behavior characteristic of a system of collective carriers in the absence of a pseudogap. The magnetic susceptibility of the underdoped samples decreases noticeably with decreasing temperature in the same range, which is typical of cuprate HTSCs in the pseudogap state [20]. However, the susceptibilities of all samples changes sharply when the temperature decreases below 120 K. The susceptibility of the most strongly doped sample (sample 1) decreases because of the closeness of the superconducting tran-

sition temperature. However, the underdoped samples, where T_c is well below the temperature range presented in Fig. 8 ($T_c = 63$ K for sample 2, $T_c = 57$ K for sample 4), exhibit paramagnetic behavior (of the Curie type) in the form of bends up in the magnetic susceptibility curves. It should be noted that this behavior in the samples cannot be related to a paramagnetic impurity, since each sample was prepared from sample 1 by changing the oxygen content (to different contents by different methods). But, sample 1 has no paramagnetic impurity (see Fig. 8).

In addition to the experimental results, Fig. 8 also shows the fitting curves calculated by Eq. (4) as the sum of contributions of various origins,

$$\chi = \chi_{\text{spin}} + C_{\text{Curie}}/T, \quad (4)$$

where

$$\chi_{\text{spin}}(T) = \mu_B^2 \langle N(\epsilon) \rangle_T, \quad (5)$$

$$\langle N(\epsilon) \rangle_T = N_0 \left\{ 1 - \left(\frac{E_g}{2T} \right)^{-1} \ln \left[\cosh \left(\frac{E_g}{2T} \right) \right] \right\}, \quad (6)$$

and N_0 is the density of states in the absence of a gap. We use the expression [20] for spin susceptibility χ_{spin} of HTSC samples in the pseudogap state. The fitting parameters were the pseudogap width (E_g) and the Curie constant (C_{Curie}). As is seen in Fig. 7, Eq. (4) well describes the magnetic susceptibility of the samples in the normal (nonsuperconducting) state. For sample 1, we have $C_{\text{Curie}} = 0$; for underdoped sample 2, we have $C_{\text{Curie}} = 115 \times 10^{-6}$ K CGS unit cm^{-3} .

We can easily show that the nature of the Curie-type paramagnetic contribution detected in these samples is related to both the occupancy of the oxygen

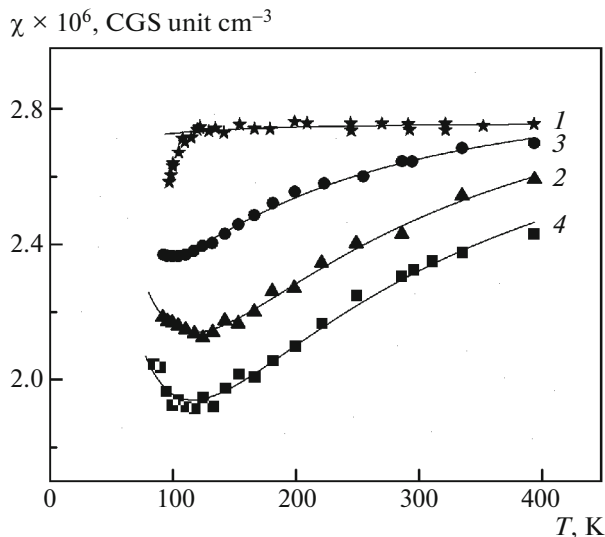


Fig. 8. Temperature dependences of the static magnetic susceptibility of equilibrium polycrystalline samples: (points) experimental data from [19] and (solid curves) calculation by Eq. (4). Numerals at the curves indicate sample numbers.

chain sites and the method of their ordering. Indeed, curves 2 and 4 in Fig. 8 correspond to samples with an almost the same oxygen content ($y \approx 6.6$). However, this oxygen index in one of them is reached by the removal of part of oxygen from the ortho phase of a Y–Ba cuprate, and this index in the other sample was reached by oxygen saturation of the tetra phase of the same compound. As a result, the values of C_{Curie} turned out to be different.

Different methods of ordering vacancies are thought to bring about different amounts of copper atoms with dangling bonds in the copper–oxygen chains. In this state, a copper atom is in the situation where one of the two nearest oxygen positions is empty. In this case, this copper atom has an uncompensated spin, which can serve as the desired Schottky center, and the number of such centers differs from the number of oxygen vacancies by 2–3 orders of magnitude, as was noted in [7].

4. CONCLUSIONS

A comparison of the results of measuring the low-temperature specific heat of polycrystalline $\text{YBa}_2\text{Cu}_3\text{O}_y$ samples with different oxygen contents or different degrees of structural disordering in magnetic fields $H = 0\text{--}9$ T and the results of measuring their static magnetic susceptibility in the temperature range $T > T_c$ showed that the paramagnetic (Schottky) centers in them were most likely to be breaks in the Cu1-O4 copper–oxygen chains, which create copper ions with uncompensated spins $s = \pm 1/2$ at the break sites. As a result of this mechanism of formation of Schottky cen-

ters, their concentration is maximal near $y \approx 6.5$ and decreases with increasing oxygen content (because of a decrease in the number of breaks in the chains). It is this behavior that was observed in our and reported experimental data (see, e.g., [2, 3]).

It is also natural to relate the increase in the degree of structural disordering in the optimally doped samples to an increase in the number of copper ions with dangling bonds in the chain plane. The absence of Schottky contributions in other cuprate HTSCs, e.g., in the LaSrCuO system, is assumed to be caused by the absence of copper–oxygen chains in their structure.

To obtain information on the nature of the Schottky anomalies in $\text{YBa}_2\text{Cu}_3\text{O}_y$, and on the method of their extraction from the experimental values of specific heat is important, since this information can be used to find other electronic contributions, which are of particular interest.

ACKNOWLEDGMENTS

We thank V.M. Pudalov for his interest in this work, V.V. Val'kov for helpful discussions, A.A. Vishnev for preparing the samples, and M.I. Ikim for the assistance.

FUNDING

This work was performed in terms of state assignment 45.22 no. 0082-2018-0003 (AAAA-A18-118012390045-2) and was supported by the Russian Foundation for Basic Research (project nos. 18-03-00528, 17-29-10016).

REFERENCES

1. N. E. Hussey, *Adv. Phys.* **51**, 1685 (2002).
2. K. A. Moller, D. L. Sisson, J. S. Urbach, et al., *Phys. Rev. B* **55**, 3954 (1997).
3. Y. Wang, B. Revaz, A. Erb, et al., *Phys. Rev. B* **63**, 094508 (2001).
4. G. E. Volovik, *JETP Lett.* **58**, 469 (1993).
5. L. G. Mamsurova, N. G. Trusevich, S. Yu. Gavrilkin, A. A. Vishnev, and L. I. Trakhtenberg, *JETP Lett.* **105**, 241 (2017).
6. L. G. Mamsurova, N. G. Trusevich, S. Yu. Gavrilkin, A. A. Vishnev and L. I. Trakhtenberg, *JETP Lett.* **106**, 378 (2017).
7. J. P. Emerson, D. A. Wright, B. F. Woodfield, et al., *Phys. Rev. Lett.* **82**, 1546 (1999).
8. S. C. Riggs, O. Vafek, J. B. Kemper, et al., *Nat. Phys.* **7**, 332 (2011).
9. K. A. Shaikhutdinov, S. I. Popkov, A. N. Lavrov, L. P. Kozeeva, M. Yu. Kameneva, V. V. Val'kov, D. M. Dzebisashvili, and A. D. Fedoseev, *JETP Lett.* **92**, 332 (2010).
10. R. A. Fisher, J. E. Gordon, and N.E. Phillips, in *Handbook of High-Temperature Superconductivity*, Ed. by

- J. R. Schrieffer and J. S. Brooks (Springer, New York, 2007), p. 345.
11. A. A. Vishnev, L. G. Mamsurova, K. S. Pigalskiy, et al., *Khim. Fiz.* **15**, 102 (1996).
 12. A. A. Vishnev, L. G. Mamsurova, K. S. Pigalskiy, et al., *Khim. Fiz.* **21**, 86 (2002).
 13. A. M. Balagurov, L. G. Mamsurova, I. A. Bobrikov, To Thanh Loan, V. Yu. Pomjakushin, K. S. Pigalskiy, N. G. Trusevich, and A. A. Vishnev, *J. Exp. Theor. Phys.* **114**, 1001 (2012).
 14. E. F. Makarov, L. G. Mamsurova, Yu. V. Permyakov, et al., *Phys. C* **415**, 29 (2004).
 15. A. A. Vishnev, E. F. Makarov, L. G. Mamsurova, K. S. Pigalskiy, and Yu. V. Permyakov, *J. Low Temp. Phys.* **30**, 275 (2004).
 16. J. L. MacManus-Driscoll, J. A. Alonso, P. C. Wang, et al., *Phys. C (Amsterdam, Neth.)* **232**, 288 (1994).
 17. Q. X. Jia, B. Maiorov, H. Wang, et al., *IEEE Trans. Appl. Supercond.* **15**, 2723 (2005).
 18. L. G. Mamsurova, K. S. Pigalskiy, N. G. Trusevich, A. A. Vishnev, M. A. Rogova, S. Yu. Gavrilkin, and A. Yu. Tsvetkov, *JETP Lett.* **102**, 662 (2015).
 19. L. G. Mamsurova, N. G. Trusevich, K. S. Pigalskiy, et al., *Bull. Russ. Acad. Sci.: Phys.* **80**, 504 (2016).
 20. S. H. Naqib, J. R. Cooper, and J. W. Loram, *Phys. Rev. B* **79**, 104519 (2009).

Translated by K. Shakhlevich